Forward and Backward Multibeam Scanning Controlled by a Holographic Acoustic Metasurface

Md Tausif Akram, Jun-Young Jang, and Kyungjun Song*
Department of Mechanical Engineering, Pusan National University, Geumjeong-Ku, Busan 46241, Republic of Korea

(Received 24 August 2021; revised 3 January 2022; accepted 11 April 2022; published 2 August 2022)

Acoustic metasurfaces have great potential in the field of beam-forming acoustic antennas due to their thin, two-dimensional, and miniature artificial materials that can freely control sound waves. Here, we propose an acoustic metasurface, with multibeam acoustic radiation serving as leaky-wave antennas used for acoustic beam steering. Based on the holographic principle, we pattern a sinusoidal modulated admittance surface, which is designed as a periodic arrangement of cylindrical holes with varying depth profiles. An omnidirectional sound generated from a tiny hole located at the center of the patterned plate creates acoustic surface waves on the modulated surface while simultaneously generating leaky-wave radiation. For multibeam steering, the holographic admittance surfaces are designed with multiple subregions of the metasurface, with each subregion emitting single-beam radiation in the desired direction. Furthermore, the holographic metasurfaces are programmed separately to have forward and backward leaky-wave radiation. In this study, we use three-dimensional additive fabrication to print acoustic holograms to craft the surface-admittance variation at subwavelength resolution. Experimental results on these printed holograms show multidirectional acoustic beam steering in close agreement with the theoretical analysis and numerical results. Forward and backward multibeam frequency scanning is also demonstrated by frequency variation. Thus, we expect that this planar surface can be used in applications such as acoustic communications, levitation, and imaging.

DOI: 10.1103/PhysRevApplied.18.024008

I. INTRODUCTION

The manipulation of sound through the use of special compact structures has been a central topic in acoustic engineering for a significant time. Recently, the concept of acoustic metasurfaces that utilize periodic array elements to manipulate sound waves was introduced. These subwavelength-thickness surfaces are used to generate local or gradient phase shifts, thus providing efficient wavefront control, aiding in the miniaturization of acoustic devices [1,2]. The unique functionalities of acoustic metasurfaces can be beneficial in a wide variety of acoustic applications, such as in acoustic lenses [3–6], beam deflectors [7], and ultrathin acoustic absorbers [8–10].

The recent surge of interest in acoustic metasurfaces in acoustic beam steering has led to the development of directional acoustic radiation apparatuses called acoustic leaky-wave antennas [11–15] (ALWAs). Leaky-wave antennas (LWAs) are initially introduced for the microwave band of electromagnetic waves [16–19] and are of significant importance in beam engineering. LWAs propagate with a designed structure, which allows for directional beam formation, analogous to phased-array antennas [20–24]. Among the different LWAs, the sinusoidal-modulated-reactance surfaces have received more attention because they independently control the leakage rate and phase constant [25,26]. Recently, an acoustic version of these sinusoidal-modulated-reactance surfaces [25] was proposed, which used a carefully designed subwavelength groove array with sinusoidal depth profiles. Therefore, high-gain ALWAs can be produced by transforming the surface waves into radiating far-field waves. The beam direction and leakage rate of sinusoidal-modulated antennas can be easily manipulated by controlling the average surface admittance, modulation period, and modulation depth [27]. In addition, an acoustic metasurface based on a sinusoidal-modulated admittance surface was developed for acoustic beam steering [28].

Furthermore, holographic acoustic antennas were recently developed by patterning a periodic array of subwavelength cylindrical holes on a base-plate surface for efficient acoustic beam steering [27,28], with the center as the feeding point, exhibiting both forward and backward surface-admittance patterning. However, this concept is limited to frequency scanning because the elevation scanning angles of the forward and backward holographic patterns are opposite, resulting in beam splitting at frequencies other than target frequency. In this study, we propose a holographic acoustic metasurface that functions as an ALWA, which can radiate in multiple directions.

*song3396@pusan.ac.kr

Different from previous methods, we design the forward and backward holographic patterns separately to realize multibeam scanning without beam splitting. Specifically, we utilize four subregions of rectangular holographic surfaces for multibeam acoustic radiation, each of which radiates single-beam radiation in a specific direction. We fabricate a holographic leaky-wave acoustic metasurface to experimentally validate the proposed method of achieving multibeam radiation. The three-dimensional (3D) prototype samples are fabricated and tested at elevation angles of 30° for a frequency of 20 kHz for both forward and backward modes to generate multibeam radiation in the targeted direction. Furthermore, frequency scanning for the forward and backward multibeam radiation is demonstrated with the change of frequency (19–21 kHz). These results show that the proposed holographic acoustic metasurface provides an excellent beam-scanning capability for multiple desired directions.

II. HOLOGRAPHIC ADMITTANCE SURFACES

The design of the holographic admittance surfaces functions as an ALWA, which is constructed by grooving a periodic array of cylindrical holes in a hexagonal pattern on a hard plastic surface, as shown in Fig. 1. Figure 1(a) shows the metasurface designed with unit cells in a hexagonal pattern, while Figs. 1(b) and 1(c) present 3D and planar views of the hexagonal-pattern unit-cell structure, respectively. An arrangement of unit cells in a hexagonal pattern is chosen to produce a surface wave in an approximately isotopically designed medium. The cylindrical grooves on the metasurface are created by varying the depth (d) of cells with the same diameter (D) and modulation periodicity (a), as illustrated in Fig. 1(c). In Fig. 1(a), the diameter of the cylindrical holes is $D = \sqrt{2}$ mm, with a periodicity of $a = 2$ mm. We obtain the dispersion curves of the acoustic surface wave by a finite element method (FEM) simulation of the unit cell. Here, the dispersion relationships are determined by implementing an eigensolver using the parametric sweep method in COMSOL Multiphysics software, and the Floquet periodic boundary condition is applied at the boundaries of the periodic unit-cell structure. Here, we consider only the dispersion in the x direction [i.e., Γ-K direction in Fig. 1(c)] due to the small anisotropy of the hexagonal unit cell on a subwavelength scale.

Figure 2(a) presents the dispersion curve of the unit cell with varying depth profiles (d). As can be seen, the surface-dispersion curves of acoustic metasurfaces depend on the value of d. For example, the larger d is, the lower the cutoff frequency of the surface wave. Furthermore, refractive-index modulation is obtained by the wave-number difference between the acoustic surface wave and free-space wave, at a given frequency. From the dispersion curves, the effective surface admittance (Y) is obtained from the refractive index, n ($n = ck_x/\omega$, where c is the sound velocity in air and k_x is the longitudinal wave number) [23,27], as follows:

$$Y = Y_0\sqrt{1 - n^2}, \tag{1}$$

where Y_0 ($Y_0 = 1/\rho c$, where ρ is the air density) denotes the free-space admittance. Equation (1) indicates that the modulated surface admittance can be easily manipulated by altering n. We control the surface-admittance value by varying the depth of the cylindrical holes arranged in a hexagonal pattern for a given frequency, which results in a variation in n along the propagation direction, leading to a change in the value of Y. Here, the surface admittance of the unit cell is generated at a frequency of 20 kHz by varying d from 1.0 to 3.75 mm.

Figure 2(b) demonstrates the surface admittance ($Y/j\,Y_0$) and refractive-index (n) profiles in blue and red, respectively, for the unit-cell structure, with respect to the

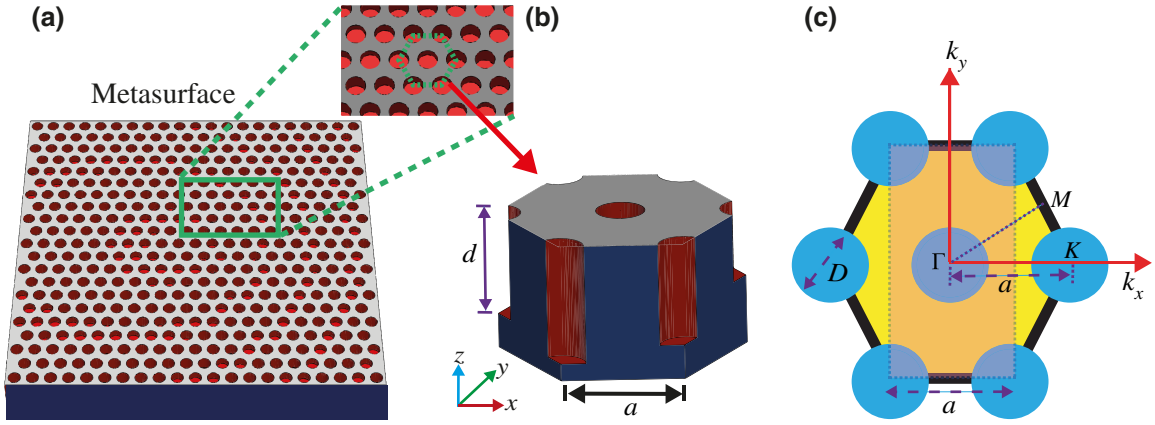

FIG. 1. (a) Schematic of the proposed metasurface with grooves arranged in a hexagonal unit-cell structure. (b) 3D view of the unit cell with varying depth (d) from 1 to 3.75 mm. (c) Planar view of the unit cell with a lattice arranged in a hexagonal pattern; rectangle in light-orange color indicates the choice of unit cell for the calculation of dispersion curves in the Γ-K direction.

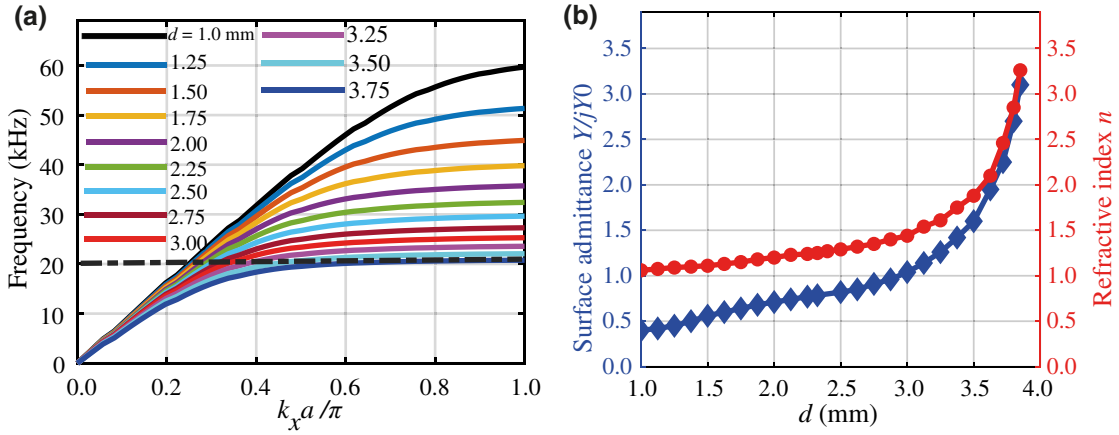

FIG. 2. (a) Dispersion curves of hexagonal unit cells with different depths of unit cell. (b) Surface admittance ($Y/j\,Y_0$) and refractive index (n) of the unit cell with varying depth profiles (d) at 20 kHz.

change in d at a frequency of 20 kHz. Figure 2(b) indicates that the values of $Y/j\,Y_0$ and n are varied from approximately 0.4 to 1.6 and 1.0 to 2.1, respectively, by changing d from 1.0 to 3.75 mm. We utilize numerical data of surface admittance to obtain the regression curve at 20 kHz as a function of d:

$$\frac{Y}{j\,Y_0} = f(d), \tag{2}$$

where $f(d)$ represents the function of d and is fitted to the five-square-root polynomial equation. Accordingly, we obtain the relationship between the surface admittance and depth, d, using a least-squares fit:

$$f(d) = -7.071 + 19.992d - 20.539d^2 + 10.17d^3 - 2.4116d^4 + 0.2211d^5. \tag{3}$$

This polynomial function can also be inverted to obtain the appropriate depth for the desired surface admittance. To utilize the ability to design the surface admittance, we pattern the holographic admittance surface using a periodic array of cylindrical holes with specific variations in the depth profiles.

III. SINGLE-BEAM STEERING BY HOLOGRAPHIC METASURAFACE

Acoustic holographic admittance surfaces are the same as electromagnetic (EM) holographic reactance surfaces, in that the directional sound beam is created by controlling the surface acoustic wave across a patterned holographic antenna [23]. According to holographic techniques, artificial surface admittances are generated by the mutual interference of the acoustic reference surface wave and object radiating wave [29,30]. Based on Eq. (3), we build two-dimensional (2D) acoustic metasurfaces by designing a periodic array of cylindrical holes in a hexagonal pattern with varying depths. Here, we consider the radiating leaky wave (object wave) for single-beam radiation at an elevation angle (θ) and azimuth angle (φ) with respect to the X-Y plane. We designate a monopole source that is placed at the origin of the acoustic holographic metasurface, which then generates an acoustic surface wave. The monopole point source is located at the center of the overall metasurface, and it is designed at a frequency of 20 kHz. Using single-beam radiation for θ and φ, the leaky-wave pressure can be defined as $\psi_{\text{rad}} = e^{-j\,\sin(\theta)k[x\,\cos(\varphi)+y\,\sin(\varphi)]}$, which will generate an interferogram with the surface wave $\psi_{\text{surf}} = e^{-jknx}$ as

$$\begin{aligned}\frac{Y}{j\,Y_0} &= Y_{\text{av}}[X + M\ \text{Re}(\psi^*_{\text{surf}}\,\psi_{\text{rad}})],\\ &= Y_{\text{av}}[X + M\ \cos(knr - kx\ \sin(\theta)\cos(\varphi)\\ &\quad - ky\ \sin(\theta)\sin(\varphi))],\end{aligned} \tag{4}$$

where k denotes the wave number ($k = 2\pi/\lambda$), r is the radial distance from the center of the metasurface, Y_{av} is the average value of the surface admittance, and M denotes the modulation depth. Here, M plays an important role in controlling the leakage rate of the holographic admittance surface. For example, a large M leads to a higher leakage rate with a larger beam width, while a small M leads to a lower leakage rate with a smaller beam width. In the design of acoustic metasurfaces, the modulated parameters $Y_{\text{av}} = 1$, $M = 0.6$, and $X = 1$ are used for holographic surface-admittance patterning. At $\theta = 30^\circ$ and $\varphi = 45^\circ$ for single-beam radiation of the holographic metasurface designed at a frequency of 20 kHz with a central feeding point, the simulation results at 20 and 19 kHz are presented in Fig. 3. The holographic metasurface with the center as a feeding point exhibits both forward and backward surface-admittance patterning. Figure 3(a) indicates

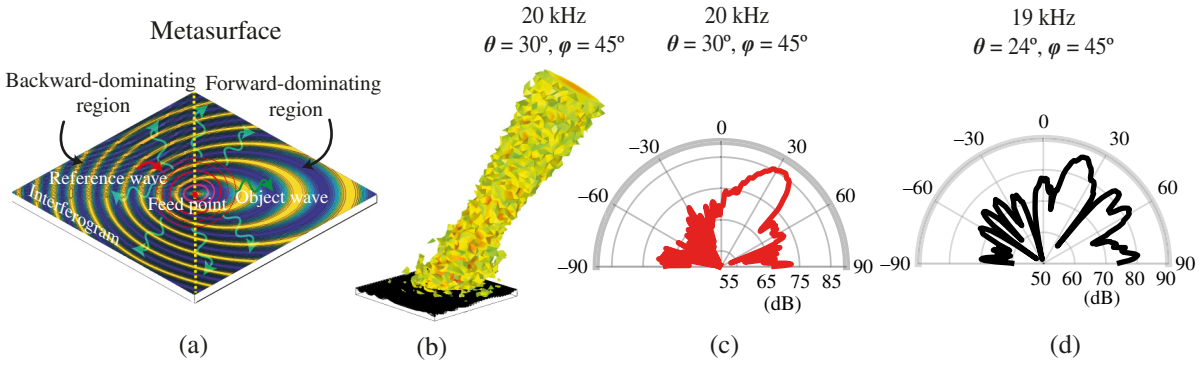

FIG. 3. (a) Holographic metasurface with a central feeding point that radiates single-beam acoustic waves; (b) bird's eye view of the simulated sound-pressure level (SPL) of a single beam at 20 kHz; results of the polar SPL in the X-Z plane are shown in (c),(d) at scanning frequencies of 20 and 19 kHz, respectively.

the direction of reference and object waves. It additionally shows the dominance of the forward and backward regions, as the feeding point is at the center of the metasurface. Figures 3(b) and 3(c) illustrate the 3D representation and polar SPL in the X-Y plane, as designed for $\theta = 30^\circ$ and $\varphi = 45^\circ$ at 20 kHz.

However, Fig. 3(d) shows that the beam pattern at 19 kHz emerging from the holographic admittance surface is similar to "rabbit ears." Beam splitting at frequencies other than the designed frequency occurs because the elevation scanning angles of forward and backward patterns are opposite. To avoid beam splitting according to operational-frequency variation, the forward and backward holographic patterns are considered separately for the frequency-scanning antennas. Detailed demonstrations for forward and backward beam-scanning properties are given in Sec. IV.

IV. FORWARD AND BACKWARD SINGLE-BEAM SCANNING BY HOLOGRAPHIC METASURFACE

In this section, forward and backward single-beam scanning of the holographic metasurface is considered. The phenomenon of frequency scanning by the 2D metasurface at $\theta = 30^\circ$ and $\varphi = 45^\circ$ with a change in frequency (19–21 kHz) is demonstrated in Figs. 4(a) and 4(b). To explain the phenomenon of frequency scanning for the forward and backward modes, it is essential to consider the longitudinal wave-number variation along with the holographic pattern according to frequency. Here, the sinusoidal phase distribution of the interference pattern is designed by $\mathrm{Re}(\psi^*_{\mathrm{surf}}\,\psi_{\mathrm{rad}})$, where $\psi_{\mathrm{surf}} = e^{-jknx}$ corresponds to the cylindrical surface wave with a wave number, k, of 20 kHz. However, the holographic admittance pattern interferes with the reference wave, ψ'_{surf}, with a different wave number, k', where k' denotes the wave number in free space ($k' = 2\pi/\lambda$) and n' is the effective refractive index. Thus, the phase, Φ, of the object wave along the holographic surface is determined by $\psi'_{\mathrm{surf}}(\psi^*_{\mathrm{surf}}\,\psi_{\mathrm{rad}})$. Here, we consider object waves as $\psi_{\mathrm{rad}} = e^{\mp j\,\sin(\theta)k[x\,\cos(\varphi)+y\,\sin(\varphi)]}$ at $\varphi = 45^\circ$ and $\theta = 30^\circ$, in which "−" and "+" signs represent the forward and backward leaky modes along the interferogram, where $x > 0$ and $y > 0$. Thus, the phase of leaky modes in the x and y direction is illustrated as

$$\Phi_x = (k'n' - kn)x \pm k\,\sin(\theta)\cos(\varphi)x \tag{5}$$

$$\Phi_y = (k'n' - kn)y \pm k\,\sin(\theta)\sin(\varphi)y \tag{6}$$

where + and − signs represent the phase of forward-radiated and backward-radiated waves, respectively, where $x > 0$ and $y > 0$. Thus, the longitudinal wave numbers in the x and y direction are given as

$$k'_{sx} = (k'n' - kn) \pm k\,\sin(\theta)\cos(\varphi), \tag{7}$$

$$k'_{sy} = (k'n' - kn) \pm k\,\sin(\theta)\sin(\varphi). \tag{8}$$

The amplitude of the longitudinal wave number is shown as

$$k'_s = \sqrt{k'^2_{sx} + k'^2_{sy}}. \tag{9}$$

Because $k'_s \le k'$, the azimuthal angle (φ') and the elevation angle (θ') of the radiation beam are expressed by

$$\varphi' = \tan^{-1}\left(\frac{k'_{sy}}{k'_{sx}}\right) \text{ and } \theta' = \sin^{-1}\left(\frac{k'_s}{k'}\right). \tag{10}$$

From the simulation results, the azimuthal angle, φ', will be unchanged with frequencies under the condition of $k'_{sx} = k'_{sy}$. As the frequency k' increases, k'_s/k' of the forward-radiating mode increases and that of the backward-radiating mode decreases. Thus, the elevation angle of the forward beam increases as frequency increases, while the elevation angle of the backward beam decreases as frequency increases.

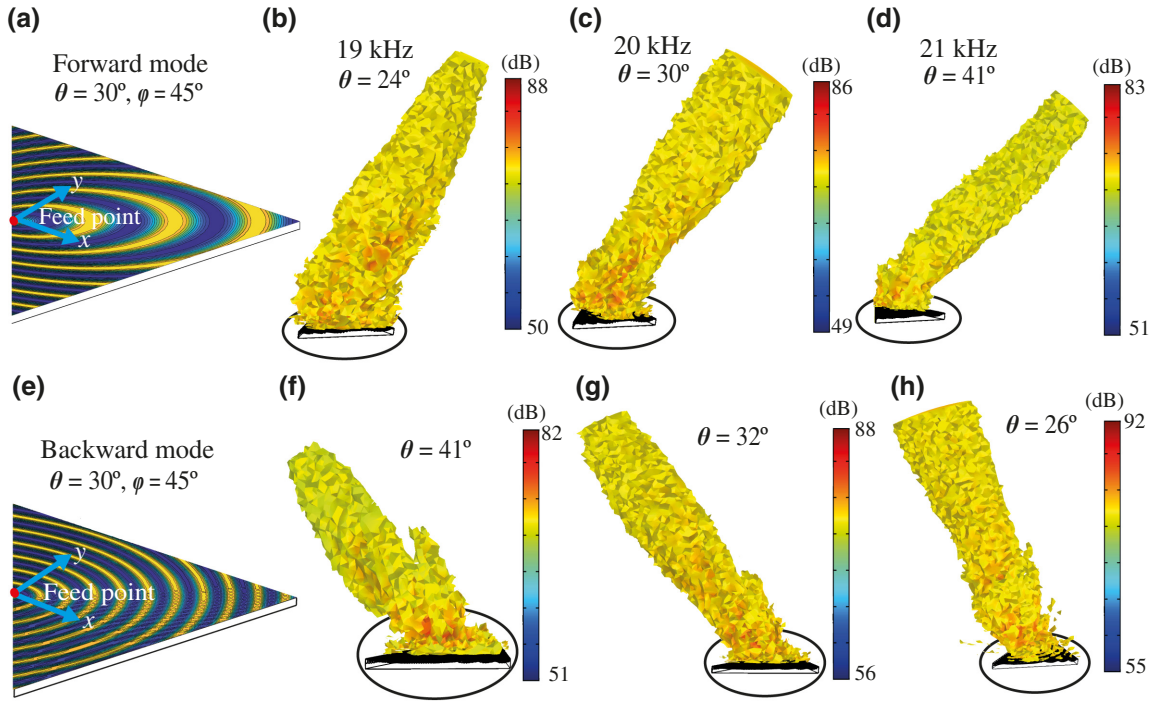

FIG. 4. (a) Proposed forward mode of holographic metasurface. (b)–(d) Frequency scanning of the single radiation beam of the forward mode with the increase in elevation angle as frequency increases. (e) Proposed backward mode of holographic metasurface. (f)–(h) Single-beam radiation of the backward mode with frequency scanning, as the elevation angle decreases with an increase in frequency. Azimuthal angle of the radiation beam is 45°.

V. FORWARD AND BACKWARD MULTIBEAM SCANNING FOR HOLOGRAPHIC ANTENNA DESIGN

For multibeam acoustic radiation, holographic admittance surfaces are designed with four acoustic metasurface subregions, each of which radiates single-beam radiation, as designated by the holographic pattern. The overall interferogram in a four-beam radiation pattern is generated by mirroring the first quadrant of the metasurface to the other quadrants. The forward leaky-wave radiation for all four quadrants of the acoustic metasurface can be theoretically described as follows:

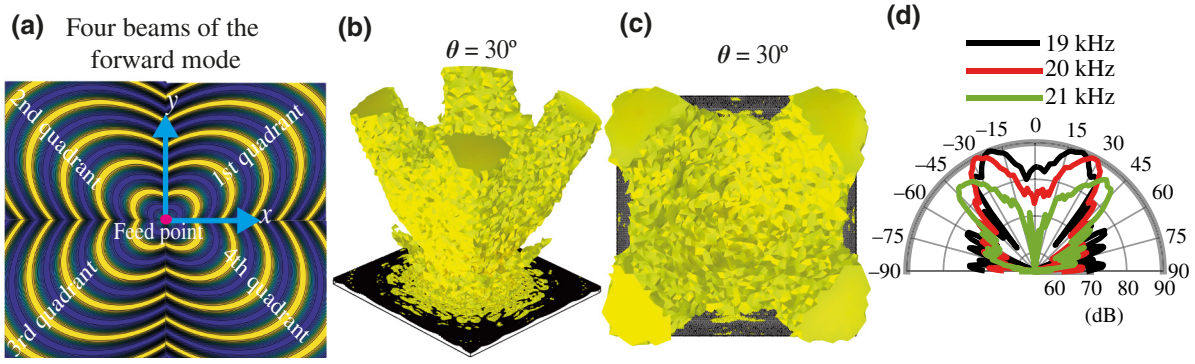

FIG. 5. (a) Metasurface prototype with elliptical contour profiles for the four beams in forward mode. 3D images of the four-beam radiation fields of the forward mode with azimuthal angles of the acoustic waves at 45°, 135°, 225°, and 315° in the first to fourth quadrants, respectively. At elevation angles of 30°, (b) bird's eye view of the acoustic waves, and (c) front view of the radiation beam. Polar SPL results in the X-Z plane are shown in (d) at frequency scanning of 19, 20, and 21 kHz.

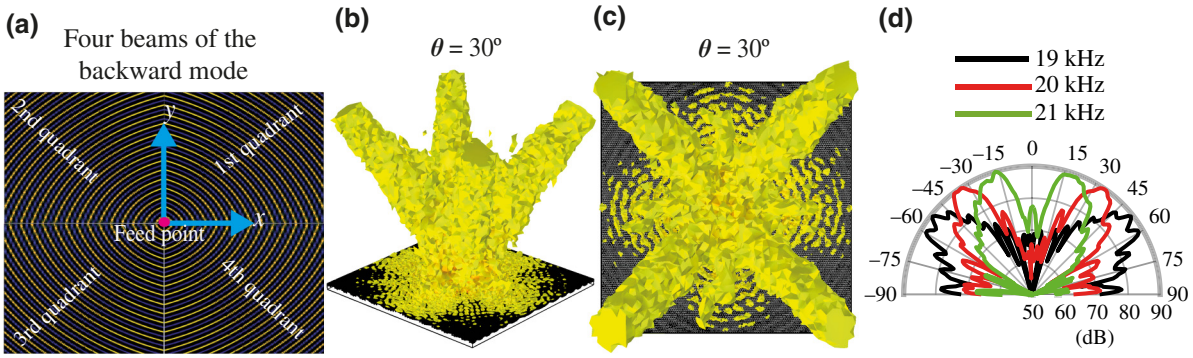

FIG. 6. (a) Proposed metasurface prototype with elliptical contour profiles for the four beams in backward mode. 3D images of the four-beam radiation fields of the backward mode with azimuthal angles of acoustic waves at 45°, 135°, 225°, and 315° in the first to fourth quadrants, respectively. For $\theta = 30°$, (b) bird's eye view of the acoustic waves, and (c) front view of the radiation beam. Polar SPL results in the X-Z plane are presented in (d) at frequency scanning of 19, 20, and 21 kHz.

$$\psi_{\text{rad}} = \begin{cases} e^{-jk\,\sin(\theta)[x\,\cos(\varphi)+y\,\sin(\varphi)]} & x>0, y>0 \quad \text{[first quadrant]}, \\ e^{-jk\,\sin(\theta)[-x\,\cos(\varphi)+y\,\sin(\varphi)]} & x<0, y>0 \quad \text{[second quadrant]}, \\ e^{-jk\,\sin(\theta)[-x\,\cos(\varphi)-y\,\sin(\varphi)]} & x<0, y<0 \quad \text{[third quadrant]}, \\ e^{-jk\,\sin(\theta)[x\,\cos(\varphi)-y\,\sin(\varphi)]} & x>0, y<0 \quad \text{[fourth quadrant]}. \end{cases} \tag{11}$$

Equation (11) represents the object wave in the forward modes for all four subareas. Consequently, multibeam radiation for all four directions of the acoustic metasurface can be obtained by exciting the surface wave, $\psi_{\text{surf}} = e^{-jknr}$, with the radiation wave (object wave) shown in Eq. (11). We determine the azimuthal angles (φ) of the four desired beams as 45°, 135°, 225°, and 315° for the first to fourth quadrants, respectively. The admittance metasurfaces are designed at elevation angles of $\theta = 30°$ with respect to the X-Y plane. The corresponding interferograms are simulated using FEM simulations for the forward mode, as shown in Fig. 5. Even though the feeding point of the overall metasurface is in the center, for each radiation beam, the subarea is being side fed. Figures 5(b) and 5(c) illustrate the 3D four-beam radiation in the forward mode at 20 kHz. The four-quadrant multibeam radiation in the forward mode is demonstrated with an elevation angle of 30°. Figure 5(d) shows the simulated results of the acoustic pressure and SPL at frequencies of 19, 20, and 21 kHz for all four quadrants of the acoustic metasurface in the X-Z

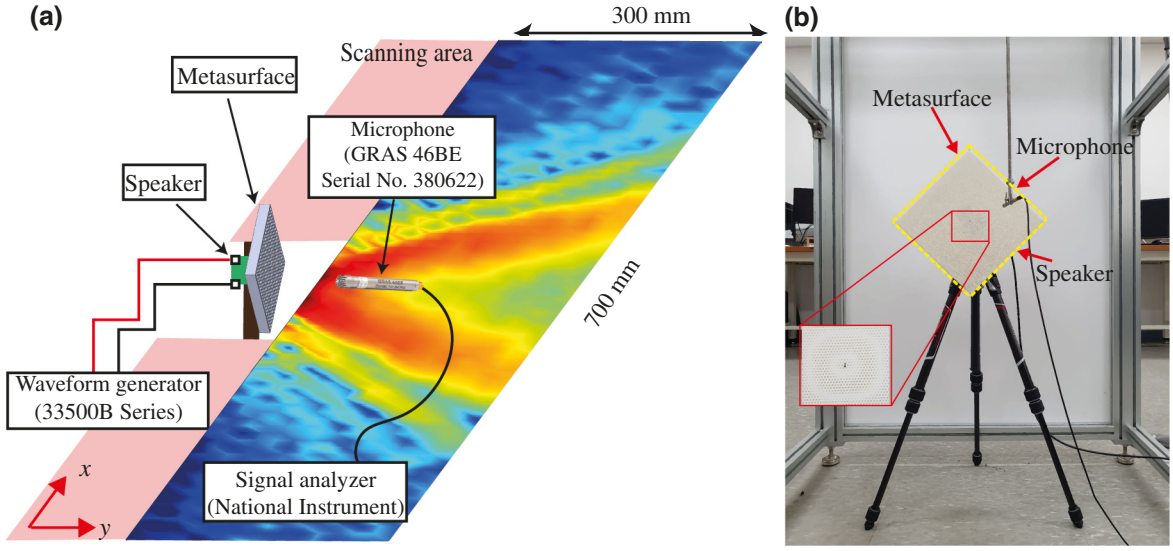

FIG. 7. (a) SPL measurement area of the beam-steering experiment. (b) Setup of experimental apparatus.

plane with respect to the surface normal of the X-Y plane. As expected, the polar plots show radiation in the forward direction at $\theta = 20°$, 30°, and 42° for scanning frequencies of 19, 20, and 21 kHz, respectively.

In addition, the 2D holographic metasurface shows four-quadrant multibeam radiation in the backward mode. The backward leaky-wave radiation for all four quadrants of the acoustic metasurface can be theoretically defined as follows:

$$\psi_{\text{rad}} = \begin{cases} e^{jk\sin(\theta)[x\cos(\varphi)+y\sin(\varphi)]} & x>0, y>0 \quad \text{[first quadrant]}, \\ e^{jk\sin(\theta)[-x\cos(\varphi)+y\sin(\varphi)]} & x<0, y>0 \quad \text{[second quadrant]}, \\ e^{jk\sin(\theta)[-x\cos(\varphi)-y\sin(\varphi)]} & x<0, y<0 \quad \text{[third quadrant]}, \\ e^{jk\sin(\theta)[x\cos(\varphi)-y\sin(\varphi)]} & x>0, y<0 \quad \text{[fourth quadrant]}. \end{cases} \tag{12}$$

Equation (12) represents the object wave in the forward modes of the leaky waves for all four subareas. Figure 6(a) shows that the holographic metasurfaces for the backward modes are designed with elevation angle $\theta = 30°$ and azimuthal angles (φ) of 45°, 135°, 225°, and 315° in the first to fourth quadrants, respectively. Figures 6(b) and 6(c) illustrate the 3D four-beam radiation in the backward mode at 20 kHz. The four-quadrant multibeam radiation in the

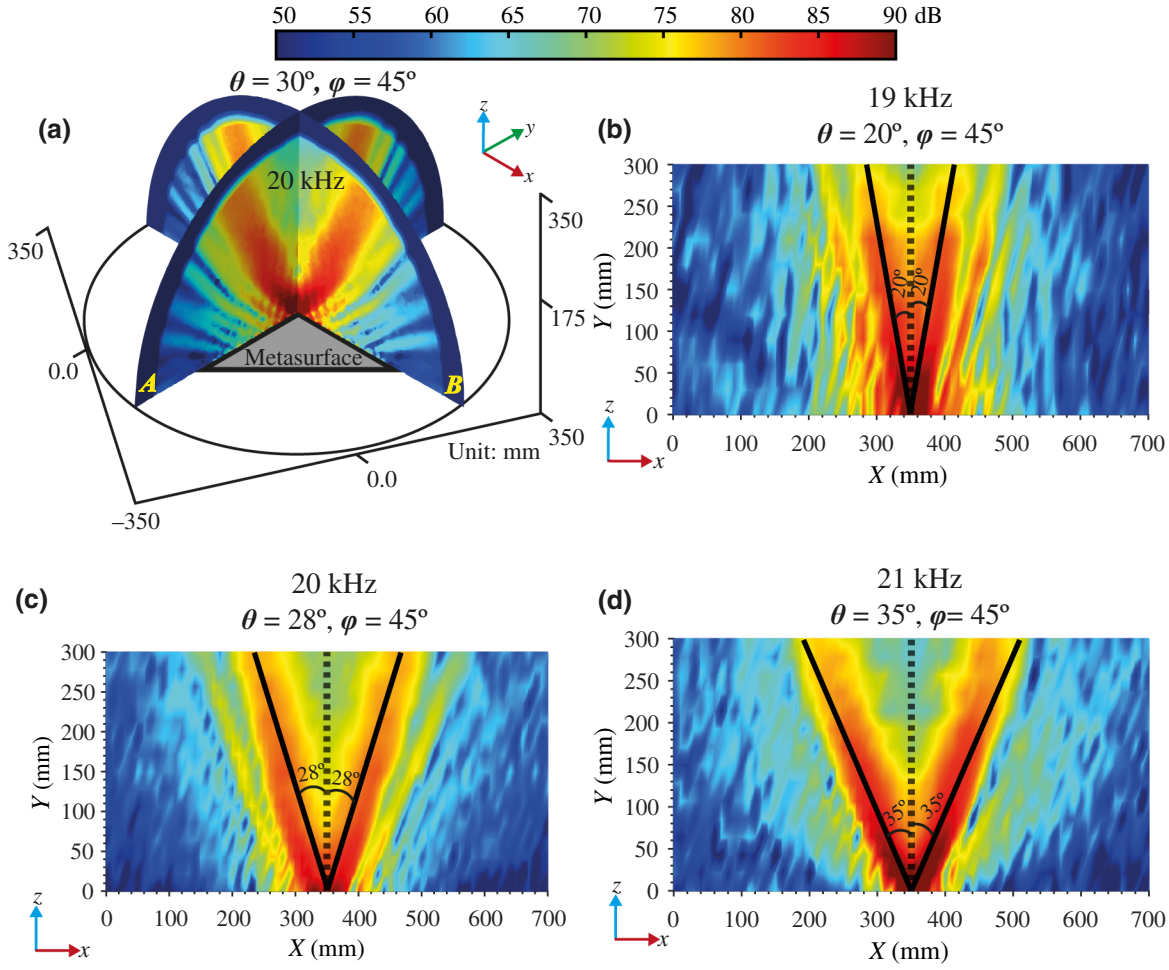

FIG. 8. (a) Simulated SPL map for the forward mode in the X-Z plane of the acoustic holographic admittance metasurface is designed to radiate acoustic waves for an elevation angle of 30° at a frequency of 20 kHz. Measured experimental SPL map generated during the process of multibeam scanning at 19, 20, and 21 kHz radiates acoustic waves at (b) 20°, (c) 28°, and (d) 35°, respectively, in reference to the surface normal.

backward mode is demonstrated with an elevation angle of 30°. Figure 6(d) presents the simulated results of the SPL of the acoustic metasurface in the X-Z plane, which shows a backward-radiation beam pattern at an angle of 46°, 32°, and 23° in all four quadrants of the acoustic metasurface, for scanning frequencies of 19, 20, and 21 kHz, respectively. Similar to single-beam scanning, as the frequency increases, the elevation angle of the forward mode becomes larger while the elevation angle of the backward mode decreases with the increase of frequency. (See the Supplemental Material [31]).

VI. EXPERIMENTAL RESULTS

Figure 7 illustrates the scanning area and experimental setup for measuring the SPL, to validate the proposed method. Here, we construct rectangular holographic admittance surfaces with cylindrical holes arranged in a hexagonal pattern. The holographic prototypes are fabricated using a Uniontech RS 450 3D printer. This type of 3D printer uses an ABS resin, acrylonitrile butadiene styrene copolymer, which is both strong and durable. The dimensions of the rectangular prototype are 240 × 240 mm^2 and it contains 14 581 cylindrical grooves.

At the center of the prototype metasurface, a small hole (1.4 mm in diameter) is drilled to emit the acoustic field generated by the miniature speaker mounted behind the hard wall of the metasurface, as illustrated in Figs. 7(a) and 7(b). For the measurement of the acoustic pressure, we assume the scan area to be 700 × 300 mm^2 in the X-Y plane, using a GRAS 46BE ¼ inch microphone with a step size of 10 mm in both the x and y directions.

The experimental results of four-beam radiation in the forward mode are demonstrated in Fig. 8. Figure 8(a) presents the FEM-simulated result of the acoustic pressure with elevation angle $\theta = 30°$ at 20 kHz, about the normal of the X-Y plane. The measured experimental SPL

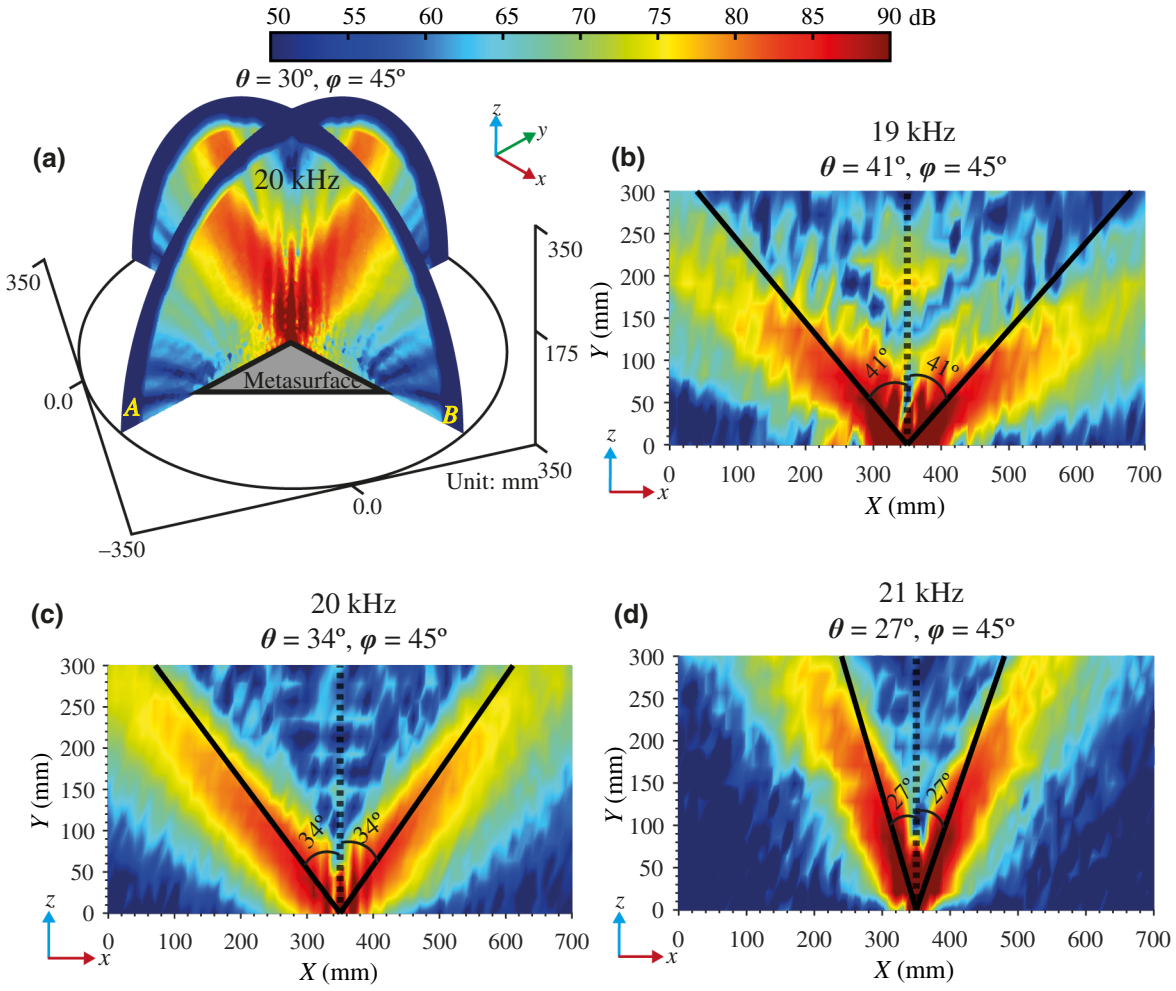

FIG. 9. (a) Simulated SPL map for the backward mode in the X-Z plane of the proposed holographic metasurface is designed to radiate four-beam radiation at an elevation angle of 30° at 20 kHz. Measured experimental SPL map generated during the process of four-beam 2D frequency scanning at 19, 20, and 21 kHz radiates acoustic waves at (b) 41°, (c) 34°, and (d) 27°, respectively, in reference to the surface normal.

results of the holographic leaky-wave metasurface for the forward-radiation mode at an elevation angle of 30° are illustrated in Figs. 8(b)–8(d). The experimental beam patterns show the directional radiation in the forward mode at $\theta = 20°$, 28°, and 35° at a frequency of 19, 20, and 21 kHz, respectively. The experimental results are in good agreement with the theoretical predictions and numerical simulations. As expected, the elevation angle, θ, increases as frequency increases. However, in the far-field environments for the forward mode, the elevation angle of beams generated during the experimental measurements are slightly deviated from the designated elevation angles. This deviation may be caused by imperfect manufacturing resolution in the 3D additive-printing process; however, this does not affect the validity of the proposed method.

The experimental results with multibeam frequency scanning in the backward mode are demonstrated in Fig. 9. Figure 9(a) shows the FEM-simulated results of the acoustic pressure for multibeam radiation in the backward mode with $\theta = 30°$ at 20 kHz. Multibeam radiation with frequency scanning of the backward radiation is shown in Figs. 9(b)–9(d). The radiation patterns illustrate the directional beam in the backward mode at $\theta = 41°$, 34°, and 27° at a frequency of 19, 20, and 21 kHz, respectively. Thus, the elevation angle, θ, decreases as frequency increases. The experimental results show a strong acoustic pressure field in the designated direction; these results are in good agreement with the simulation results and the theoretical prediction.

VII. CONCLUSION

In this study, we present the theoretical design, numerical simulation, fabrication, and experimental verification of holographic acoustic metasurfaces for multibeam scanning. Based on sinusoidal holographic surface admittance, ALWAs have the potential to steer a beam of radiation in all possible directions. Both numerical and experimental results show efficient forward and backward radiation in multiple designated directions. ALWAs provide the directional leaky waves at $\theta = 30°$ with the desired φ of the four beams of 45°, 135°, 225°, and 315°, respectively, for 20 kHz. Forward and backward multibeam radiation with frequency scanning is also demonstrated by operating-frequency variation. Furthermore, it is extended to active beam steering by incorporating actuators to reconfigure the design parameters of the holographic metasurface. Thus, the proposed design has potential applications in small acoustic radar systems, such as acoustic speakers, sonar, and ultrasonic devices [31].

ACKNOWLEDGMENTS

This work is supported by the Center for Advanced Meta-Materials (CAMM) funded by the Ministry of Science and ICT as part of the Global Frontier Project (CAMM Grant No. 2019M3A6B3031048) and the National Research Foundation of Korea (NRF) funded by the Ministry of Education (Grant No. NRF-2020R1F1A1074404).

[1] N. Yu, P. Genevet, M. A. Kats, F. Aieta, J.-P. Tetienne, F. Capasso, and Z. Gaburro, Light propagation with phase discontinuities: Generalized laws of reflection and refraction, Science **334**, 333 (2011).
[2] B. Assouar, B. Liang, Y. Wu, Y. Li, J.-C. Cheng, and Y. Jing. Acoustic metasurfaces, Nat. Rev. Mater. **3**, 460 (2018).
[3] Y. Li, G. Yu, B. Liang, X. Zou, G. Li, S. Cheng, and J. Cheng, Three-dimensional ultrathin planar lenses by acoustic metamaterials, Sci. Rep. **4**, 6830 (2015).
[4] K. Song, J. Kim, S. Hur, J.-H. Kwak, S.-H. Lee, and T. Kim, Directional reflective surface formed via gradient-impeding acoustic meta-surfaces, Sci. Rep. **6**, 32300 (2016).
[5] Y.-F. Zhu, X.-Y. Zou, R.-Q. Li, X. Jiang, J. Tu, B. Liang, and J.-C. Cheng, Dispersionless manipulation of reflected acoustic wavefront by subwavelength corrugated surface, Sci. Rep. **5**, 10966 (2015).
[6] X.-D. Fan, Y.-F. Zhu, B. Liang, J. Yang, and J.-C. Cheng, Broadband convergence of acoustic energy with binary reflected phases on planar surface, Appl. Phys. Lett. **109**, 243501 (2016).
[7] B. Xie, K. Tang, H. Cheng, Z. Liu, S. Chen, and J. Tian, Coding acoustic metasurfaces, Adv. Mater. **29**, 1603507 (2017).
[8] J. Mei, G. Ma, M. Yang, Z. Yang, W. Wen, and P. Sheng, Dark acoustic metamaterials as super absorbers for low-frequency sound, Nat. Commun. **3**, 756 (2012).
[9] Y. Li and B. M. Assouar, Acoustic metasurface-based perfect absorber with deep subwavelength thickness, Appl. Phys. Lett. **108**, 063502 (2016).
[10] S. Huang, X. Fang, X. Wang, B. Assouar, Q. Cheng, and Y. Li, Acoustic perfect absorbers via spiral metasurfaces with embedded apertures, Appl. Phys. Lett. **113**, 233501 (2018).
[11] H. Esfahlani, S. Karkar, H. Lissek, and J. R. Mosig. Acoustic dispersive prism, Sci. Rep. **6**, 18911 (2016).
[12] H. Esfahlani, S. Karkar, H. Lissek, and J. R. Mosig, Exploiting the leaky-wave properties of transmission-line metamaterials for single-microphone direction finding, J. Acoust. Soc. Am. **139**, 3259 (2016).
[13] C. J. Naify, M. D. Guild, C. A. Rohde, D. C. Calvo, and G. J. Orris, Demonstration of a directional sonic prism in two dimensions using an air-acoustic leaky wave antenna, Appl. Phys. Lett. **107**, 133505 (2015).
[14] C. J. Naify, C. N. Layman, T. P. Martin, M. Nicholas, D. C. Calvo, and G. J. Orris, Experimental realization of a variable index transmission line metamaterial as an acoustic leaky-wave antenna, Appl. Phys. Lett. **102**, 203508 (2013).
[15] K. Song, K. Kim, S. Hur, J.-H. Kwak, J. Park, J. R. Yoon, and J. Kim, Sound pressure level gain in an acoustic metamaterial cavity, Sci. Rep. **4**, 7421 (2015).
[16] R. A. Shelby, D. R. Smith, S. C. Nemat-Nasser, and S. Schultz, Microwave transmission through a

two-dimensional, isotropic, left-handed metamaterial, Appl. Phys. Lett. **78**, 489 (2001).

[17] D. R. Smith, W. J. Padilla, D. C. Vier, S. C. Nemat-Nasser, and S. Schultz, Composite Medium with Simultaneously Negative Permeability and Permittivity, Phys. Rev. Lett. **84**, 4184 (2000).

[18] J. B. Pendry, Negative Refraction Makes a Perfect Lens, Phys. Rev. Lett. **85**, 3966 (2000).

[19] J. Liu, T. Su, B. Wu, and H. Lv, Holographic design of leaky-wave antenna with gain controlled four beams, Microw. Opt. Technol. Lett. **61**, mop. 31637 (2018).

[20] D. F. Sievenpiper, Forward and backward leaky wave radiation with large effective aperture from an electronically tunable textured surface, IEEE Trans. Antennas Propag. **53**, 236 (2005).

[21] C. Caloz and T. Itoh, Transmission line approach of left-handed (LH) materials and microstrip implementation of an artificial LH transmission line, IEEE Trans. Antennas Propag. **52**, 1159 (2004).

[22] G. V. Eleftheriades, O. Siddiqui, and A. K. Iyer, Transmission line models for negative refractive index media and associated implementations without excess resonators, IEEE Microw. Wireless Comp. Lett. **13**, 51 (2003).

[23] B. H. Fong, J. S. Colburn, J. J. Ottusch, J. L. Visher, and D. F. Sievenpiper, Scalar and tensor holographic artificial impedance surfaces, IEEE Trans. Antennas Propag. **58**, 3212 (2010).

[24] Y. Zhu, J. Hu, X. Fan, J. Yang, B. Liang, X. Zhu, and J. Cheng, Fine manipulation of sound via lossy metamaterials with independent and arbitrary reflection amplitude and phase, Nat. Commun. **9**, 1632 (2018).

[25] A. M. Patel and A. Grbic, A printed leaky-wave antenna based on a sinusoidally-modulated reactance surface, IEEE Trans. Antennas Propag. **59**, 2087 (2011).

[26] K. Song, Md. Anzan-Uz-Zaman, J.-H. Kwak, J.-Y. Jung, J. Kim, and S. Hur, Concentric artificial impedance surface for directional sound beamforming, AIP Adv. **7**, 035315 (2017).

[27] K. Song, J.-H. Kwak, J. J. Park, S. Hur, Md. Anzan-Uz-Zaman, and J. Kim, Acoustic Beam Forming Based on a Surface with Sinusoidally Modulated Admittance, Phys. Rev. Appl. **10**, 044025 (2018).

[28] J. Kim, S. Park, Md. Anzan-Uz-Zaman, and K. Song, Holographic acoustic admittance surface for acoustic beam steering, Appl. Phys. Lett. **115**, 193501 (2019).

[29] Y. B. Li, X. Wan, B. G. Cai, Q. Cheng, and T. J. Cui, Frequency-controls of electromagnetic multi-beam scanning by metasurfaces, Sci. Rep. **4**, 6921 (2015).

[30] Y. Zhu, N. J. Gerard, X. Xia, G. C. Stevenson, L. Cao, S. Fan, C. M. Spadaccini, Y. Jing, and B. Assouar, Systematic design and experimental demonstration of transmission-type multiplexed acoustic metaholograms, Adv. Funct. Mater. **31**, 2101947 (2021).

[31] See the Supplemental Material at http://link.aps.org/supplemental/10.1103/PhysRevApplied.18.024008 for multibeam scanning results for both forward and backward mode for the azimuthal angle 30°, 150°, 210°, and 330°.